THE ASTRONOMICAL JOURNAL, 116:2032–2041, 1998 October
© 1998. The American Astronomical Society. All rights reserved. Printed in U.S.A.

THE YARKOVSKY SEASONAL EFFECT ON ASTEROIDAL FRAGMENTS: A NONLINEARIZED THEORY FOR THE PLANE-PARALLEL CASE

D. VOKROUHLICKÝ
Astronomical Institute, Charles University, V Holešovičkách 2, CZ–180 00, Praha 8, The Czech Republic
AND
P. FARINELLA
Dipartimento di Matematica, Università di Pisa, via Buonarroti 2, I-56127 Pisa, Italy
Received 1998 May 8; revised 1998 July 2

ABSTRACT

The "seasonal" Yarkovsky force is due to radiation pressure recoil, which acts on anisotropically emitting rotating bodies, heated by sunlight to different temperatures at different latitudes on their surfaces. This force gives rise to a significant draglike effect on rapidly spinning asteroid fragments $\approx$1–100 m in size. Here we present a new treatment of this effect, based on the numerical solution of the heat transfer equation with no linearization in the ratio between the peak temperature difference and the average temperature on the body's surface. Our treatment is restricted to the large-body (plane-parallel) case, valid for radii larger than the penetration depth of the seasonal thermal wave ($\approx$1–20 m depending on the conductivity of the surface layer). Also, we solve numerically the Gaussian perturbation equations for the evolution of the orbital eccentricity, as well of the semimajor axis under the seasonal Yarkovsky force. We find the results to be in broad agreement with the linearized model of D. P. Rubincam, with two main discrepancies: (i) for the same thermal and optical parameters and near-circular orbits, the semimajor axis decay rate predicted by the improved, nonlinearized theory is some 15% lower, and (ii) for some directions of the spin axis relative to the perihelion direction, the Yarkovsky force can cause a secular growth of the eccentricity. When gravitationally induced perihelion precession, spin axis precession, and collisional reorientations are accounted for, however, the eccentricity on average is found to decrease. We also show that the theory can be easily generalized to bodies of spheroidal shapes, with typical discrepancies of a factor of 2 in the semimajor axis decay rate with respect to the spherical case.

Key words: meteors, meteoroids — minor planets, asteroids

1. INTRODUCTION

The dynamics of bodies orbiting in the solar system is generally considered as the paradigm of an N-body gravitational problem and, as such, has been the main playing field of classical celestial mechanics for the last three centuries. The predominance of gravitation over all the other forces has been interpreted as the distinctive feature of celestial mechanics with respect to its terrestrial counterpart and has both led to an unprecedented accuracy in the "deterministic" predictions of the future and allowed the study of subtle chaotic and/or resonant effects.

On the other hand, in the last few decades the relevance of nongravitational forces for orbiting objects, both manmade (Milani, Nobili, & Farinella 1987) and natural (Kaula 1966; Burns, Lamy, & Soter 1979), has become apparent. This is obvious for microscopic dust particles, whose motion is strongly affected by radiation pressure, electromagnetic effects, Poynting-Robertson drag, and solar wind; but the orbital evolution of larger bodies can also be dominated in the very long term by nongravitational effects, thanks to the conservative nature of gravitational forces that in many cases results in nearly constant orbital semimajor axes. The classical example of a small dissipative process leading to important long-term consequences is that of tidal forces in planet-satellite systems. Less known—although also discovered long ago—is the so-called Yarkovsky effect, the radiation pressure recoil that acts on anisotropically emitting spinning bodies, heated by sunlight to different temperatures on different parts of their surfaces (Öpik 1951; Radzievskii 1952; Peterson 1976; Burns et al. 1979; Afonso, Gomes, & Florczak 1995). Recently, following related work on laser-tracked artificial satellites (e.g., Rubincam 1987; Farinella & Vokrouhlický 1996), a "seasonal" variant of the Yarkovsky effect has been proposed by Rubincam (1995, 1998) to be effective for fragments $\approx$1–100 m in size in transporting them from their source regions in the main asteroid belt (or Mars) to the Earth's vicinity. We have also proposed that Yarkovsky-driven semimajor axis drift is important in delivering collisionally generated asteroid fragments to the resonant zones of the orbital element space in the inner part of the main belt, whence most meteorites and near-Earth asteroids are believed to come (Farinella, Vokrouhlický, & Hartmann 1998; Vokrouhlický & Farinella 1998; Hartmann et al. 1997).

This paper is devoted to refining the available models for the seasonal Yarkovsky effect, from several points of view. First, we give up the approximation in which only linear terms in the ratio between surface temperature changes and average temperature are retained in the fragment thermal models. Second, we investigate in some detail the Yarkovsky effect on other orbital elements besides the semimajor axis, taking into account the presence of planetary perturbations and spin axis precession. Third, we generalize the theory to spheroidal shapes, in order to assess the sensitivity of the results to the usual assumption of a spherical fragment shape.

The remainder of this paper is organized as follows. In § 2 we review the physics of the seasonal Yarkovsky effect and summarize some previous work on this subject. Section 3 is devoted to developing a suitable quantitative model for the thermal response of an asteroid fragment to the solar radi-

ation influx and the corresponding perturbing force affecting its orbit. In § 4 we discuss the resulting orbital effects in a number of specific cases, and in § 5 we summarize the main conclusions from our work and the current open problems.

2. MODELING THE YARKOVSKY SEASONAL EFFECT: ASSUMPTIONS AND APPROXIMATIONS

Solar radiation heats anisotropically the surface of any orbiting solar system body. If the body rotates and the response to external heating is not instantaneous, because of a finite time lag for the conduction of part of the absorbed energy to the interior of the body, a rather involved thermal model must be developed to determine the surface temperature distribution. So far, this has been done mainly for the purpose of determining asteroid diameters with the radiometric technique (e.g., Brown & Matson 1987; Lebofsky & Spencer 1989; Spencer, Lebofsky, & Sykes 1989). However, as a by-product of the surface temperature gradients, the thermal radiation emitted from the warmer parts of the surface carries away more linear momentum than that emitted from the cooler regions. The overall momentum budget results in a net *thermal force* affecting the orbital motion, as was first suggested by I. O. Yarkovsky about one century ago (see the references listed in § 1).

From the study of similar problems in the context of artificial satellite dynamics (e.g., Rubincam 1987, 1988; Slabinski 1997; Farinella & Vokrouhlický 1996), it has been realized that the main features of the thermal perturbations are determined by the ratio between the thermal relaxation time $t_{\rm rel}$ (the characteristic timescale for the thermal response of the body to an external excitation) and the rotation period $t_{\rm rot}$ (this ratio is the thermal parameter Θ, which plays a crucial role in the formulation of thermal models; see § 3). If the relaxation time is comparable, or smaller, than the rotation period, the longitudinal component of the temperature gradients on the surface is significant, and the resulting force has components perpendicular to the spin axis. This is the classical, or "diurnal," Yarkovsky force that is important for bodies with a relatively slow rotation or small thermal inertia (see Peterson 1976; Farinella et al. 1998; Vokrouhlický 1998a). On the contrary, if the thermal relaxation time is much longer than the rotation period (as is the case for the *LAGEOS* artificial satellite), the longitudinal temperature gradients on the surface are averaged out, leaving only the latitudinal component, so that the thermal force tends to be aligned with the spin axis. This is the seasonal variant of the Yarkovsky force that we are going to model in this paper. As discussed by Rubincam (1995, 1998), Farinella et al. (1998), and Vokrouhlický & Farinella (1998), the seasonal effect is probably more important for asteroidal fragments in the diameter range from a few meters to ≈ 100 m, provided their surfaces are *not* covered by an insulating regolith layer and they do not have exceedingly slow rotations. This effect is inherently nonlocal, as the thermal response to solar heating occurs at a significantly shifted position along the orbit. This feature has important dynamical consequences, in particular, because it gives rise to a draglike dissipative effect ("thermal drag") that always shrinks the orbital semimajor axis.

Both the diurnal and the seasonal Yarkovsky effects work in a very different way for "large" and "small" bodies. The transition size is related to the typical depth reached by the thermal wave (the region where the temperature varies periodically) over the timescale of the external energy influx. This timescale is of course $t_{\rm rot}$ for the diurnal effect and $t_{\rm rev}$ (the orbital period) for the seasonal effect. In the large-body case, the object can be modeled as a flat plane of infinite depth, with no thermal communication between its opposite sides; on the contrary, in the small-body case, the entire interior of the body is affected by the thermal wave and the thermal gradients are damped down. As stressed by Rubincam (1998), the seasonal effect is maximum near the transition size, because larger bodies are less sensitive to nongravitational effects due to their small area-to-mass ratio, whereas smaller bodies become more and more isothermal. In this paper, we are going to deal with the large-body case only; that is, we shall use a thermal model suited to the plane-parallel approximation. Note that in the case of the seasonal effect we can still introduce the thermal parameter Θ_n defined above, provided we compare the thermal relaxation time $t_{\rm rel}$ to the orbital period $t_{\rm rev} = 2\pi/n$ (n being the orbital mean motion) instead of the spin period $t_{\rm rot}$. We have

$$\Theta_n = \frac{t_{\rm rel}}{t_{\rm rev}} = \frac{\Gamma\sqrt{n}}{\epsilon\sigma T^3}\,, \tag{1}$$

where $\Gamma = (K\rho C_p)^{1/2}$ is the thermal inertia, ϵ is the infrared emissivity of the surface, σ is the Stefan-Boltzmann constant, and T is the mean surface temperature (this may be estimated in different ways, resulting in numerical discrepancies by factors of order unity between thermal parameters defined by different authors). The index n reminds us that we are dealing with the seasonal Yarkovsky effect.

As discussed by Rubincam (1998) and Farinella et al. (1998), the transition between the small- and large-body regimes occurs at radii of about 10 and 30 m for rocky and metal-rich fragments, respectively. This can be seen as follows. Suppose that a given surface element of the body undergoes an external radiative heating characterized by a typical frequency ν. Then, the solution of the heat diffusion problem (e.g., Wesselink 1948; Spencer et al. 1989) suggests that the temperature response decays exponentially in the surface layer of the body with a characteristic length l_S:

$$l_S \simeq \sqrt{\frac{K}{\rho\nu C_p}}\,, \tag{2}$$

where K is the mean thermal conductivity, ρ is the density, and C_p is the specific heat of the body (or its surface layer). Below this depth, the temperature is almost unaffected by the surface processes. A given body (such as an asteroidal fragment) is "large" provided that its radius $R_A > l_S$. Using the thermal parameters of basalt as reported by Rubincam (1995), i.e., $K \simeq 2.65$ W m^{-1} K^{-1}, $C_p \simeq 680$ J kg^{-1} K^{-1} and $\rho \simeq 3500$ kg m^{-3} (similar values have been found for silicates, see Peterson 1976 and Burns et al. 1979; for chondrites the conductivity can be up to factor of 5 lower, see Yomogida & Matsui 1983), and the seasonal frequency n, we obtain that l_S is about 10 m.

3. THERMAL MODEL AND YARKOVSKY FORCE

3.1. *Reference Frames*

We are going to use the orbital elements of a fragment's orbit defined in an inertial reference system. Three auxiliary unit vectors can be associated to the mean orbit, namely,

the vector $\boldsymbol{n}$ normal to it,

$$\boldsymbol{n} = \begin{pmatrix} \sin I \sin \Omega \\ -\sin I \cos \Omega \\ \cos I \end{pmatrix}; \quad (3)$$

the vector $\boldsymbol{P}$ directed toward the mean pericenter,

$$\boldsymbol{P} = \begin{pmatrix} \cos \Omega \cos \omega - \cos I \sin \Omega \sin \omega \\ \sin \Omega \cos \omega + \cos I \cos \Omega \sin \omega \\ \sin I \sin \omega \end{pmatrix}; \quad (4)$$

and the vector $\boldsymbol{Q}$ lying in the mean orbital plane and defined by $\boldsymbol{Q} = \boldsymbol{n} \times \boldsymbol{P}$. In the previous equations, the mean inclination I, the mean longitude of ascending node Ω, and the mean argument of pericenter ω appear. We shall use the orbit-related reference frame having the x-axis along the direction of $\boldsymbol{P}$ and the z-axis along the direction of $\boldsymbol{n}$ (Beletskii 1975).

To derive the thermal force effects on the fragment's mean orbit, we need to define two other geometric quantities related to the $\boldsymbol{s}$ unit vector directed along the spin axis: (i) the obliquity angle γ, defined in the interval 0 to π, between $\boldsymbol{s}$ and $\boldsymbol{n}$, i.e., $\cos \gamma = \boldsymbol{s} \cdot \boldsymbol{n}$; and (ii) the "longitude" $\hat{\omega}$ of the projection of the spin axis onto the mean orbital plane, defined in the orbit-related reference frame, that is,

$$s_P = (\boldsymbol{s} \cdot \boldsymbol{P}) = \sin \gamma \sin \hat{\omega}\,, \quad (5a)$$

$$s_Q = (\boldsymbol{s} \cdot \boldsymbol{Q}) = \sin \gamma \cos \hat{\omega}\,. \quad (5b)$$

The angles γ and $\hat{\omega}$ can be interpreted as spherical angles—colatitude and longitude—of the fragment's spin axis vector $\boldsymbol{s}$ in a reference system defined by the unit vectors ($\boldsymbol{P}$, $\boldsymbol{Q}$, $\boldsymbol{n}$). Figure 1 illustrates the geometrical quantities introduced above.

Since, in general, the orbit of the fragment undergoes planetary perturbations and the mean orientation of the spin axis is changed by both precession and collisions, neither γ nor $\hat{\omega}$ is constant. The indirect effects, due to planetary perturbations of the fragment orbit, dominate the evolution of (γ, $\hat{\omega}$) on a timescale of 10^4–10^5 yr, whereas on longer times Yarkovsky effects themselves should be accounted for. The direct terms include both "free" and forced precession (the latter due to the solar gravitational field), while collisions are caused by the flux of small asteroidal and cometary debris (Farinella et al. 1998). We will assess the precessional effects in § 4, although we are not going to analyze in detail collisional effects here. Collisions can be approximated as a sequence of random, instantaneous steps in the orientation of $\boldsymbol{s}$. As shown by Farinella et al. (1998), impacts imparting an angular momentum sufficient to cause a complete reorientation of the spin axis typically occur at intervals of 10^6–10^7 yr for fast-rotating, meter-sized fragments. Therefore, collisions can be neglected over times much shorter than this, whereas over much longer times their random character is consistent with assuming an isotropical distribution of spin axis orientations in computing averaged Yarkovsky effects.

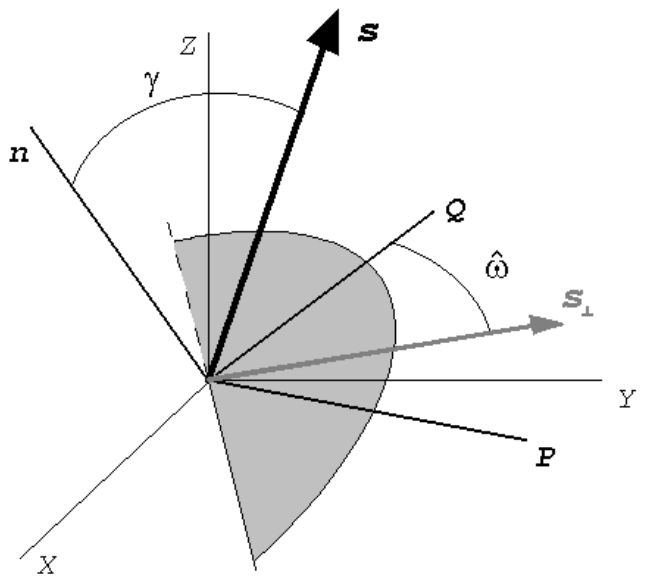

FIG. 1.—The two reference systems used in this paper: (i) the inertial system (XYZ) to which mean orbital elements are referred, and (ii) the orbit-related system (xyz) defined by the orbital angular momentum unit vector $\boldsymbol{n}$ and the pericenter unit vector $\boldsymbol{P}$. Projections of the spin vector $\boldsymbol{s}$ in the latter system define the geometrical parameters γ and $\hat{\omega}$.

3.2. *Spherical Fragments*

In this section we describe the thermal model of asteroidal fragments that will be used to compute the Yarkovsky force. It is based on a fully numerical method, similar to that used in Spencer et al. (1989). For the sake of simplicity, we start by assuming a spherical shape, although later on we will discuss how to generalize our model to spheroidal bodies (§ 3.3). We always assume that the body is homogeneous, with a given set of physical and thermal constants.

Since the asteroidal fragments that we deal with are "large" bodies, in the sense defined in § 2, we are allowed to use a planar approximation of the heat diffusion problem (Spencer et al. 1989). Also, the "large" size of the body ensures that the thermal histories of different surface elements are not correlated to each other. Therefore, we shall start by formulating the heat diffusion problem for the temperature evolution in an infinitely deep surface layer below a chosen surface element. Denoting the local vertical coordinate by x (oriented downward) and time by t, the local temperature $T(t, x)$ must fulfill the heat equation (see, e.g., Landau & Lifschitz 1986)

$$\rho C_p \frac{\partial T}{\partial t} = K \frac{\partial^2 T}{\partial x^2}\,, \quad (6)$$

with boundary conditions

$$\epsilon \sigma T^4(t, 0) = K\left(\frac{\partial T}{\partial x}\right)(t, 0) + \alpha \mathscr{E}(t)\,, \quad (7a)$$

$$\left(\frac{\partial T}{\partial x}\right)(t, \infty) = 0\,. \quad (7b)$$

Here α is the surface absorption coefficient in the visible band and $\mathscr{E}(t)$ is the radiation flux into the surface element. The former equation expresses the energy balance on the surface, while the latter means that at large depths the temperature is unaffected by any external illumination.

In § 2 we pointed out a second important assumption in our study, that is, that the fast rotation of the fragment results in a constant temperature for all the surface elements at the same colatitude θ (the angle from the spin axis). As a consequence, we can average equations (6), and (7a) and (7b) over a rotation period. Thus, we assume that T

depends on time t and depth x as before, and to keep track of the seasonal temperature variations, we add explicitly the dependence on θ. Equations (6) and (7b) remain formally unchanged, whereas equation (7a) now reads

$$\epsilon\sigma T^4(t, 0; \theta) = K\left(\frac{\partial T}{\partial x}\right)(t, 0; \theta) + \alpha\bar{\mathscr{E}}(t; \theta) , \quad (8)$$

with the averaged radiation flux at a given latitude given by

$$\bar{\mathscr{E}}(t; \theta) = \frac{\Phi}{\pi}(\sin\theta \sin\theta_0 \sin\phi_* + \phi_* \cos\theta \cos\theta_0) , \quad (9)$$

with the auxiliary angle ϕ_* defined as

$$\cos\phi_* = \begin{cases} -1 & \text{for } \theta < \theta_- , \\ -\cot\theta \cot\theta_0 & \text{for } \theta \in (\theta_-, \theta_+) , \\ 1 & \text{for } \theta > \theta_+ . \end{cases} \quad (10)$$

Here we defined $\theta_\pm \equiv \pi/2 \pm \theta_0$, with θ_0 the solar colatitude in the fragment's system. The scalar quantity Φ represents the solar radiation flux at the distance of the fragment. The solar colatitude θ_0 depends on time and can be expressed as

$$\cos\theta_0 = -\sin\gamma \sin w , \quad (11)$$

with $w = \hat{\omega} + v$, v being the true anomaly of the body.

In order to write simpler equations, we follow Spencer et al. (1989) in defining nondimensional variables as follows. The local vertical coordinate x is scaled by the thermal length l_S, the depth of the thermal wave with a frequency ν equal to the orbital mean motion n (see § 2). Thus, we have $x \to X = x/l_S$. Instead of time t, we use the fragment's mean orbital longitude ℓ: $t \to \ell = n(t - t_0)$, with t_0 corresponding to perihelion passage. The mean radiation flux $\bar{\mathscr{E}}(t; \theta)$ is scaled by the solar radiation flux at the mean semimajor axis distance: $\bar{\mathscr{E}} \to \bar{\mathscr{E}}' = \bar{\mathscr{E}}/\Phi_a$. Here $\Phi_a = \mathscr{C}/a^2$, with $\mathscr{C}$ denoting the solar constant and a the mean semimajor axis in Astronomical Units (hereafter, a will always be treated as a nondimensional quantity). Finally, the temperature is scaled by effective subsolar temperature T_{ss} at the mean semimajor axis distance from the radiation source: $T \to T' = T/T_{ss}$, with T_{ss} defined by the relationship $\epsilon\sigma T_{ss}^4 = \alpha\Phi_a$.

The heat diffusion problem in the new set of variables is then expressed by the following parabolic differential equation:

$$\frac{\partial T'}{\partial \ell} = \frac{\partial^2 T'}{\partial X^2} , \quad (12)$$

with the boundary conditions

$$T'^4(\ell, 0; \theta) = \Theta_n\left(\frac{\partial T'}{\partial X}\right)(\ell, 0; \theta) + \bar{\mathscr{E}}'(\ell; \theta) , \quad (13a)$$

$$\left(\frac{\partial T'}{\partial X}\right)(\ell, 0; \theta) = 0 . \quad (13b)$$

The mean energy influx at a given latitude can be written as

$$\bar{\mathscr{E}}'(\ell; \theta) = \frac{\psi}{\pi}(\sin\theta \sin\theta_0 \sin\phi_* + \phi_* \cos\theta \cos\theta_0) , \quad (14)$$

with

$$\psi(\ell) = \left(\frac{1 + e\cos v}{1 - e^2}\right)^2 . \quad (15)$$

The auxiliary angles ϕ_* and $\theta_\pm$ are the same as defined before (see eq. [10]).

We are now ready to introduce the set of basic parameters that define the thermal model. The only physical coefficient entering equations (12) and (13) is the thermal parameter Θ_n (see eq. [1]). Recalling the dependence of the subsolar temperature T_{ss} on the mean orbital elements, we shall explicitly write $\Theta_n = \Theta_0 a^{3/4}$, splitting the thermal parameter into a *constant* part Θ_0 and an orbit-dependent part. The former term, Θ_0, depends only on the thermal properties of the fragment, the radiation flux, and the scaling factor for the mean semimajor axis a. As 1 AU has been chosen for the latter quantity, we may alternatively state that Θ_0 is the value of the thermal parameter at this distance from the Sun. Assuming regolith-free surfaces and using the material constants of basalt, we obtain $\Theta_0 \simeq 0.32$, whereas for metal-rich fragments we have $\Theta_0 \simeq 1.62$. As for the orbital and rotational parameters, the thermal model depends on the mean orbital semimajor axis a and eccentricity e, plus the two angles γ and $\hat{\omega}$, as defined earlier. All of these parameters in general are time dependent.

Equations (12) and (13), with the heating function (14), can now be solved numerically using a method very similar to that described in detail by Spencer et al. (1989). We recall that the thermal inertia of the fragments is supposed to be large enough that there is a considerable time lag between heating at a given latitude and the corresponding temperature response. Thus, for a given set of mean elements we can solve separately for the temperature history at any given latitude along an entire orbital revolution. Typically, we use 2000 steps in the anomaly ℓ, along with 40 nodes in the scaled vertical coordinate X, and we need 50–100 iterations to converge to a solution of equations (12) and (13) within a tolerance of 10^{-6}; the entire procedure is repeated for 250 values of $\cos\theta$ between -1 and 1 to obtain the surface temperature distribution. We impose the periodicity of the solution after one revolution, which is justified because the mean orbital elements evolve on a timescale much longer than one orbital period (provided there are no close encounters of the fragment with one of the major bodies in the solar system and/or collisions with other fragments). This calculation takes a computing time of the order of a few minutes on a workstation.

Once the heat diffusion problem is solved and we dispose of the "seasonal" temperature distribution $T'(\ell, 0; \theta)$ on the fragment's surface at any "time" ℓ during one revolution, we can directly compute the resulting thermal force. Since the rotation is assumed to be fast, the only nonzero component of the thermal acceleration is $a_S(\ell)$, directed along the spin axis and depending on ℓ; that is,

$$a_S(\ell) = -\frac{4\alpha}{3}\frac{\mathscr{A}_r}{a^2}\int_{-1}^{1} d(\cos\theta) T'^4(\ell; \theta)\cos\theta$$

$$\equiv \frac{4\alpha}{3}\frac{\mathscr{A}_r}{a^2} A(\ell) . \quad (16)$$

This integral is also computed numerically. The order of magnitude of a_S is given by the usual radiation force param-

eter $\mathscr{A}_r \equiv \pi R_A^2 \mathscr{C}/Mc \simeq 3\mathscr{C}/4R_A c\rho$ (here c is the velocity of light), which is scaled by the integral factor $A(\ell)$. If we consider an object with $R_A \simeq 50$ m and $\rho \simeq 3500$ kg m^{-3} (basalt), we obtain $\mathscr{A}_r \simeq 2 \times 10^{-11}$ ms^{-2}. Note that, in agreement with the results of Rubincam (1995, 1998), smaller fragments drift faster than larger ones, since $\mathscr{A}_r \propto 1/R_A$. Of course, this is true only as long as the large-body regime can be assumed to hold, as was discussed in § 2 (see also Rubincam 1998).

In order to describe the long-term evolution of the orbit, we have to choose a suitable set of mean orbital elements. Since according to Rubincam (1995) the thermal force typically leads to the circularization of orbits, to avoid problems with near-circular orbits, we use the following set of nonsingular elements: mean semimajor axis a, normal vector $\boldsymbol{n}$ to the mean orbital plane, and three components of the Lenz vector $\boldsymbol{K}$ of the mean orbit. We normalize the Lenz vector, so that $\boldsymbol{K} \equiv e\boldsymbol{P}$, where e is the mean orbit eccentricity and $\boldsymbol{P}$ is the pericenter vector as defined before. Only five variables are independent, because of the two constraints $\boldsymbol{n} \cdot \boldsymbol{n} = 1$, $\boldsymbol{n} \cdot \boldsymbol{K} = 0$.

Now we have to average the right-hand sides of the Gaussian perturbation equations (see, e.g., Bertotti & Farinella 1990, chap. 11) in order to get the long-term variations of the mean orbital elements caused by the Yarkovsky effect. Simple algebra yields

$$\left(\frac{da}{d\chi}\right)_t = \frac{2}{\eta\sqrt{a}} \{[e(\beta + \beta_{cc}) + (1 + e^2)\beta_c]s_Q - (\beta_s + e\beta_{sc})s_P\} , \tag{17a}$$

$$\left(\frac{d\boldsymbol{n}}{d\chi}\right)_t = \frac{\eta s_n}{a\sqrt{a}} (-\beta_c \boldsymbol{Q} + \beta_s \boldsymbol{P}) , \tag{17b}$$

$$\left(\frac{d\boldsymbol{K}}{d\chi}\right)_t = -\frac{\eta}{a\sqrt{a}} \{[\beta_{sc} s_P - (\beta + \beta_{cc} + 2e\beta_c)s_Q]\boldsymbol{P} + [(2\beta - \beta_{cc} + e\beta_c)s_P - (\beta_{sc} + e\beta_s)s_Q]\boldsymbol{Q} + e\beta_s \boldsymbol{s}\} , \tag{17c}$$

with

$$\beta = \left\langle \frac{A(\ell)}{1 + e\cos v} \right\rangle ,$$

$$\beta_s = \left\langle \frac{A(\ell)\sin v}{1 + e\cos v} \right\rangle , \quad \beta_c = \left\langle \frac{A(\ell)\cos v}{1 + e\cos v} \right\rangle ,$$

$$\beta_{sc} = \left\langle \frac{A(\ell)\sin v\cos v}{1 + e\cos v} \right\rangle , \quad \beta_{cc} = \left\langle \frac{A(\ell)\cos^2 v}{1 + e\cos v} \right\rangle .$$

Here the brackets indicate that an average over one revolution (with ℓ as a variable) has to be done, and $\eta \equiv (1 - e^2)^{1/2}$. This average in our approach is performed numerically, after renormalizing the time variable according to $\chi = \kappa(t - t_0)$, with

$$\kappa = \frac{4\alpha}{3} \frac{\mathscr{A}_r}{n_1 R_1} , \tag{18}$$

n_1 being the mean motion of a body orbiting at a distance $R_1 = 1$ AU from the Sun. The inverse of κ corresponds to the characteristic timescale over which thermal effects modify the orbit. Considering $\mathscr{A}_r \simeq 2 \times 10^{-11}$ms^{-2} as in the previous example, with $\alpha \simeq 0.9$ we obtain $\kappa^{-1} \simeq 40$ Myr.

The most significant feature of the orbit evolution process caused by the Yarkovsky force is a slow semimajor axis decay, according to equation (17a). The eccentricity evolution resulting from the Lenz vector dynamics expressed by equation (17c) can be written as

$$\left(\frac{de}{d\chi}\right)_t = \boldsymbol{P} \cdot \left(\frac{d\boldsymbol{K}}{d\chi}\right)_t = \frac{\eta}{a\sqrt{a}} [(\beta + \beta_{cc} + 2e\beta_c)s_Q - (\beta_{sc} + e\beta_s)s_P] . \tag{19}$$

This equation is also relevant for solar system applications, for at least two reasons: first, high eccentricities can cause orbital crossings with the inner planets even for bodies with main-belt values of a, and second, Rabinowitz's (1993, 1994) recent discovery of a population of near-Earth bodies, 10–100 m in size, with fairly low eccentricities. We will discuss the eccentricity evolution in some detail in the next section. Note, however, that whenever $\beta > 0$ and $\beta_{cc} > 0$, there is the possibility that the Yarkovsky-driven evolution pumps up the eccentricity, provided the initial e is small and $s_P \simeq 0$. A similar argument does not apply to the semimajor axis equation (17a), because the coefficient $(\beta_s + e\beta_{sc}) = \langle A \sin v \rangle$ vanishes when $s_Q \simeq 0$. Indeed, our numerical results show that thermal effects always decrease the orbital energy (that is, $da/dt < 0$) for any reasonable orbital parameters.

For circular orbits, we have the obvious symmetry $T'(\ell; \theta) = T'(\ell + \pi; \pi - \theta)$, due to the fact that the temperature histories at latitudes symmetric with respect to the body's equator are shifted by half a revolution. Then we have $\beta = \beta_{cc} = \beta_{sc} = 0$, and therefore $(de/dt)|_{e=0} \propto e$. This result agrees with those of Rubincam (1995, 1998).

Finally, an obvious feature of the seasonal Yarkovsky effect is that equations (17a)–(17c) are invariant under the inversion of the spin axis orientation ($\boldsymbol{s} \to -\boldsymbol{s}$), since in this case all the β quantities change their sign.

Of course, so far we have neglected the fact that besides the Yarkovsky effects expressed by equations (17a)–(17c), planetary perturbations also affect the mean orbital elements of asteroid fragments. These perturbations typically act over shorter timescales, 10^4–10^6 yr, so it is somewhat artificial to consider thermal effects independently of them. However, the nonconservative character of the Yarkovsky effect, resulting in a significant semimajor axis decay, is an essential difference between the two types of perturbations. Therefore, at least as far as we are mainly concerned with the semimajor axis evolution, we can separate gravitational and Yarkovsky-driven perturbations.

3.3. *Generalization to Spheroidal Bodies*

We are now going to generalize the previous results to the case of bodies of spheroidal shape rotating around their axis of symmetry (or having a small nutation angle; see Vokrouhlický 1998b for some basic geometrical results about the ellipsoids of rotation). The ratio of the polar radius $R_{A,p}$ to the equatorial radius $R_{A,e}$ of the bodies will be denoted by $\varepsilon = R_{A,p}/R_{A,e}$. We discuss both oblate ($\varepsilon < 1$) and prolate ($\varepsilon > 1$) spheroids (similar thermal models for ellipsoidal bodies have been discussed by Brown 1985, Lagerros 1996, and Vokrouhlický 1998b, where the results

have been applied to the diurnal Yarkovsky effect). Interestingly, only minor modifications of the previous formulation are needed. In particular, the averaged heating function (14) now reads

$$\bar{\mathscr{E}}'(\ell;\theta)=\frac{\psi}{\pi J_4(\theta)}(\varepsilon^2\sin\theta\sin\theta_0\sin\phi_*+\phi_*\cos\theta\cos\theta_0)\,, \tag{20}$$

with a modified definition of the auxiliary angle ϕ_*:

$$\cos\phi_*=\begin{cases}-1 & \text{for } \theta<\theta_-\,,\\ -\varepsilon^{-2}\cot\theta\cot\theta_0 & \text{for } \theta\in(\theta_-,\theta_+)\,,\\ 1 & \text{for } \theta>\theta_+\,.\end{cases} \tag{21}$$

Similarly, the $\theta_\pm$ latitude angles are now given by $\cot\theta_\pm=\mp\varepsilon^2\tan\theta_0$. It is also useful to introduce the auxiliary functions ($n=1, 2, \ldots$)

$$J_n(\theta)=\sqrt{\varepsilon^n\sin^2\theta+\cos^2\theta}\,. \tag{22}$$

The spin axis–oriented thermal acceleration (16) in this case becomes

$$a_S(\ell)=-\frac{4\alpha}{3}\frac{\mathscr{A}_r}{a^2}\int_{-1}^{1}d(\cos\theta)\,\frac{\cos\theta}{J_2^4(\theta)}\,T'^4(\ell;\theta)\,, \tag{23}$$

where $\mathscr{A}_r\equiv\pi R_{A,p}^2\mathscr{C}/Mc$. Apart from these modifications, our method and results are unchanged.

4. EXAMPLES

4.1. *Preliminary Tests*

As the secular orbital decay is the most distinctive feature of the seasonal Yarkovsky effect, we first assess the dependence of the averaged transverse acceleration component $\langle T\rangle$ on the mean semimajor axis a. Rubincam (1995), who developed a linearized model for the thermal response to external heating in the plane-parallel geometry (large-body case), obtained for circular orbits the analytical result

$$\langle T\rangle_R\propto-\frac{\Phi_1}{1+2\Phi_1+2\Phi_1^2}\left(\frac{\sin\gamma}{a}\right)^2\,, \tag{24}$$

where $\Phi_1=\Theta_n/2\propto a^{3/4}$ (see Rubincam 1995). Depending on the proportionality constant of this relationship, we have two extreme cases: (1) if $\Phi_1\ll 1$, we have approximately $\langle T\rangle_R\propto a^{-5/4}$, which is a good match to the behavior of regolith-free basaltic fragments; and (2) if instead $\Phi_1\gg 1$, we get $\langle T\rangle_R\propto a^{-11/4}$, which holds approximately for metal-rich fragments (both cases are shown in Fig. 3 of Rubincam 1995). We remind the reader that in all cases the transverse force decreases slower than the diurnal Yarkovsky effect (DY), for which we have $\langle T\rangle_{\rm DY}\propto a^{-7/2}$ (Radzievskii 1952; Peterson 1976; Vokrouhlický 1998a).

On the other hand, our formula for the averaged transverse force component is more complex:

$$\langle T\rangle\propto-\frac{1}{a^2}\int_{-1}^{1}d(\cos\theta)\,\frac{\cos\theta}{J_2^4(\theta)}\times\langle(s_Q\cos v-s_P\sin v)T'^4(\ell;\theta;\Theta_n)\rangle\,, \tag{25}$$

where we have evidenced the functional dependence of the temperature solution on the thermal parameter $\Theta_n\propto a^{3/4}$. There is also a "hidden" dependence of $\langle T\rangle$ on e and γ through the dependence of the heating function $\bar{\mathscr{E}}'$ on the solar latitude θ_0, which, in turn, depends on $\sin\gamma$ as given by equation (11), and the dependence of ψ on the eccentricity as given by equation (15).

Of course, the dependence of the orbit-averaged quantities, such as $\langle T\rangle$, on the parameter $\hat{\omega}$ disappears for circular orbits. Thus, in this case we can set $\hat{\omega}=0$ without loss of generality. Then, if we try to fit the relationship between $\langle T\rangle$ and a with a power law, $\langle T\rangle\propto a^m$, in the basalt case ($\Theta_0=0.32$) and assuming $\sin\gamma=1$, we obtain $m=-1.623\pm0.012$. This confirms the slow decrease of the seasonal Yarkovsky effect for increasing orbital radii. On the other hand, in the metal case ($\Theta_0\simeq 2$), we obtain $m=-2.124\pm0.007$. Figure 2 shows the dependence of $\langle T\rangle$ on a in both cases, assuming circular orbits and the spin axis in the orbital plane. We see that the draglike effect on metal-rich objects decays much faster for increasing distances from the Sun, in agreement with the findings of Rubincam (1995).

Figure 3 shows the mean transverse accelerations (24) and (25) for circular orbits of radius $a=1$ AU, as a function of Θ_0 (or, equivalently, Φ_1 in Rubincam's notations; this figure should be compared with Fig. 3 in Rubincam 1995). Recall that $\Theta_0\propto\Gamma$, so that small values of Θ_0 correspond to lower thermal inertias (and vice versa). The results in Figures 2 and 3 suggest that Rubincam's (1995) linear solution somewhat overestimates the mean Yarkovsky drag, as expected by Rubincam himself, who applied (e.g., in his Figs. 4 and 5) a 25% reduction to his estimated accelerations to account for nonlinear effects. Actually, we verified in detail Rubincam's remark (see the Appendix of his paper) that the linear approximation smears a bit the temperature variations over one revolution, but it overestimates significantly the thermal lag between the maximum radiation heating and the maximum amplitude of the Yarkovsky force. The net result is a somewhat larger average force in the linear approximation than from our nonlinearized approach. At $\Theta_0\simeq 1.62$ and $\gamma=90°$, the discrepancy is about 15%, and it grows slightly at lower obliquities. This is due to the fact that the dependence of $\langle T\rangle$ on γ is somewhat steeper than in Rubincam's theory. If we fit to our results a power-law relationship such as $\langle T\rangle\propto\sin^m\gamma$, we obtain (in

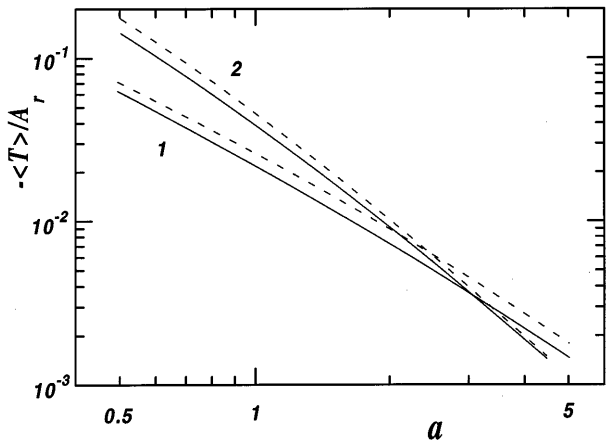

FIG. 2.—Averaged along-track component of the seasonal Yarkovsky acceleration $-\langle T\rangle/\mathscr{A}_r$ vs. orbital distance a (in AU) from the Sun. Circular orbits and spin axis in the orbital plane ($\gamma=90°$) have been assumed. Two types of material have been considered: (1) basalt, with $\Theta_0\simeq 0.32$, and (2) metal, with $\Theta_0\simeq 1.62$. The solid lines correspond to the nonlinearized (numerical) solution of this paper, the dashed lines to the linear (analytical) solution of Rubincam (1995).

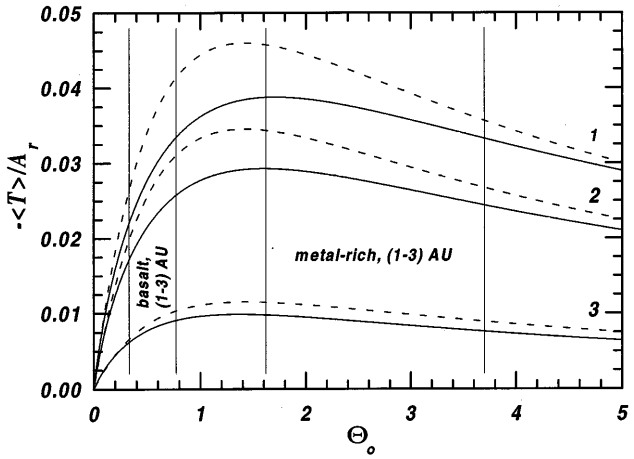

FIG. 3.—Plot of $-\langle T\rangle/\mathscr{A}_r$ vs. the thermal parameter $\Theta_0(\propto\Gamma)$. Circular orbits at $a = 1$ AU are assumed. Different obliquity angles γ have been considered: (1) $\gamma = 90°$, (2) $\gamma = 60°$, and (3) $\gamma = 30°$. The solid lines correspond to the nonlinearized (numerical) solution of this paper, the dashed lines to the linear (analytical) solution of Rubincam (1995). The typical ranges of values of Θ_0, in both the basalt and the metal-rich case and for orbital radii ranging from 1 to 3 AU, are also shown.

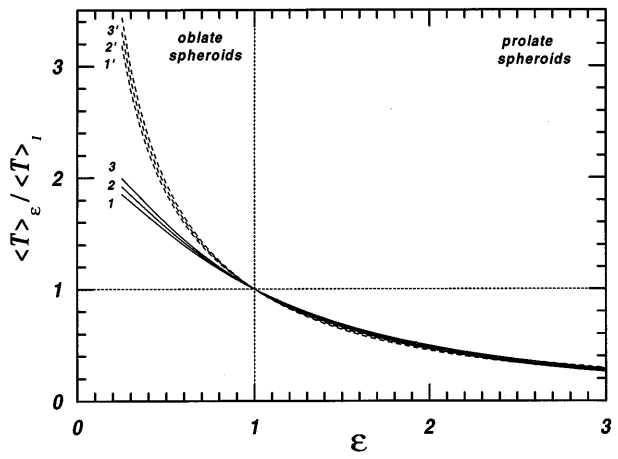

FIG. 4.—The ratio $\langle T\rangle_\varepsilon/\langle T\rangle_1$ of the seasonal Yarkovsky along-track accelerations for flattened and spherical bodies, vs. the flattening parameter $\varepsilon = R_{A,p}/R_{A,e}$. Two methods are used to perform this comparison: (i) objects having the same mass (*dashed curves*), and (ii) objects having the same ratio between the mean cross section with respect to the Sun and mass (*solid curves*). In each case, three different values of the thermal parameter Θ_n have been assumed: (1) $\Theta_n = 0.32$, (2) $\Theta_n = 1$, and (3) $\Theta_n = 2$.

the basalt, circular-orbit case) $m = 1.956 \pm 0.006$, to be compared with Rubincam's result $\langle T\rangle_R \propto \sin^2\gamma$.

Next, we compare the effects on spherical and spheroidal objects, the latter characterized by a flattening parameter ε. Assuming again $\gamma = 90°$ and circular orbits ($e = 0$), we compare objects with the same mean ratio between the geometric cross section in the direction of the Sun and mass. If $\mathscr{J}$ denotes the integral on the right-hand side of equation (25), we obtain

$$\frac{\langle T\rangle_\varepsilon}{\langle T\rangle_1} = \sigma(\varepsilon)\,\frac{\mathscr{J}_\varepsilon}{\mathscr{J}_1}\,, \tag{26}$$

with the function $\sigma(\varepsilon)$ given by

$$\sigma(\varepsilon) = \frac{\pi}{2}\,\frac{\varepsilon^2}{E(\sqrt{1-\varepsilon^2})} \qquad \text{for } \varepsilon < 1\,, \tag{27a}$$

$$\sigma(\varepsilon) = \frac{\pi}{2}\,\frac{\varepsilon}{E(\sqrt{1-1/\varepsilon^2})} \qquad \text{for } \varepsilon > 1\,, \tag{27b}$$

where $E(m)$ is the complete elliptic integral of the second kind. Equation (27b) can be obtained from equation (27a) by the use of the complex transformation of the elliptic functions (see, e.g., Vokrouhlický 1998b). The subscript "ε" indicates that the corresponding quantity has been computed for a spheroid with flattening ε, while the subscript "1" indicates the same variable computed for a spherical body ($\varepsilon = 1$). If we choose a different way of comparing spherical and flattened bodies, equation (26) would still hold, but with a different $\sigma(\varepsilon)$ correspondence function. For instance, if we compare objects with the same mass, we have simply $\sigma(\varepsilon) = \varepsilon^{4/3}$. Figure 4 shows the ratio (26) for different values of the thermal parameter Θ_n and the two comparison methods mentioned above. Because of the relation $\Theta_n \propto \Theta_0\, a^{3/4}$, we can interpret these curves as corresponding to different materials or to different mean distances from the Sun. The figure shows that for moderate values of ε, say, between 0.5 and 2, the draglike acceleration changes by a factor of the order of 2 with respect to the spherical case and even more for more extreme shapes. Of course, real fragments have more irregular (e.g., triaxial) shapes than simple spheroids, but typically their axial ratios are of the order of 2 (see, e.g., Catullo et al. 1984; Giblin et al. 1994), and we can expect that the discrepancies with respect to the idealized spherical case are about the same as for the spheroids.

4.2. *Yarkovsky Seasonal Effect for Planar Orbits*

To investigate the orbital evolution of fragments under the Yarkovsky seasonal effect, we first deal with a simplified case. We neglect planetary perturbations and assume that the spin axis of the fragment lies in the orbital plane and keeps a constant direction. In this case, $\gamma \equiv 90°$ and $s_n \equiv 0$; we arbitrarily choose $\boldsymbol{s} = (1, 0, 0)^T$. Equation (17b) then gives $\boldsymbol{n} =$ constant, namely, a constant orientation of the orbital plane, as expected. In this case, we can simplify our notations by choosing the reference system so that $\boldsymbol{n} = (0, 0, 1)^T$, leaving only two nontrivial components K_1 and K_2 of the Lenz vector. In a similar way, the vectors $\boldsymbol{P} = (P_1, P_2, 0)^T$ and $\boldsymbol{Q} = (-P_2, P_1, 0)^T$ have only two nontrivial components in the XY reference plane, and the orbital eccentricity can be expressed as $e = |K| = (K_1^2 + K_2^2)^{1/2}$. The longitude of pericenter ϖ and the parameter $\hat{\omega}$ can be easily obtained by the relationships $(K_1, K_2) = e(\cos\varpi, \sin\varpi) = e(\sin\hat{\omega}, -\cos\hat{\omega})$. The dynamical equations for the three independent variables (a, K_1, K_2) read

$$e\eta\left(\frac{da}{d\chi}\right)_t = -\frac{2}{\sqrt{a}}\,\{(\beta_s + e\beta_{sc})K_1 + [e(\beta + \beta_{cc}) + (1 + e^2)\beta_c]K_2\}\,, \tag{28a}$$

$$\frac{e^2}{\eta}\left(\frac{dK_1}{d\chi}\right)_t = -\frac{1}{a\sqrt{a}}\,[(\beta_{sc} + e\beta_s)K_1^2 + (2\beta_{cc} - \beta + e\beta_c)K_1K_2 - \beta_{sc}K_2^2]\,, \tag{28b}$$

$$\frac{e^2}{\eta}\left(\frac{dK_2}{d\chi}\right)_t = -\frac{1}{a\sqrt{a}}\,[(\beta - \beta_{cc})K_1^2 + (2\beta_{sc} + e\beta_s)K_1K_2 + (\beta_{cc} + e\beta_c)K_2^2 + \beta + e\beta_c]\,. \tag{28c}$$

Note that here all the β quantities depend on semimajor axis a and eccentricity e through their dependence on the

thermal force integral $A(\ell)$. Therefore, this system of equations is highly nonlinear and has been integrated numerically. There is a symmetry that helps in limiting the range of pericenter longitudes to be considered: if $(a; K_1, K_2)$ is a solution of equations (28a)–(28c), then $(a; -K_1, -K_2)$ is also a solution (note that when $\varpi \to \varpi + \pi$, the β quantities change their sign).

To integrate equations (28a)–(28c), we have selected the following initial conditions: $a = 2.5$ AU, $e = 0.25$, and ϖ in the range (0°, 180°). Figure 5 illustrates the results for a set of fictitious bodies, with each curve corresponding to an object with a different initial value of ϖ). All bodies are assumed to be regolith-free basalt spheres of radius $R_A = 50$ m. The ticks along the curves correspond to intervals of 250 Myr. Of course, for smaller objects, the orbital evolution would be faster (see the discussion in § 3.2). Several conclusions can be drawn from these results.

As for the rate of semimajor axis decrease, we confirm the result of Rubincam (1995) that a time of the order of 0.5–1 Gyr is required to bring fragments 50 m in radius from the main asteroid belt to a Mars-crossing orbit. Interestingly enough, the semimajor axis decay process is almost independent of the particular value of $\hat{\omega}$ and can be approximately expressed by a simple relation of the form $a(0) - a(\chi) \propto \chi^{0.98}$.

A novel result of our approach concerns the behavior of the eccentricity. Whereas linearized models such as those discussed by Rubincam (1995, 1998) indicate that the seasonal Yarkovsky effect should always circularize orbits, we find that both secular increases and decreases of the eccentricity are possible, depending on the initial position of the pericenter. Actually, despite the fact that the value of the eccentricity derivative (19) averaged over the entire range of pericenter arguments is always negative, inspection of Figure 5 would suggest a mean tendency to increase the eccentricity. The reason for this is the following: whenever we do not "force" the pericenter argument to circulate, due to planetary and other perturbations (as it will be discussed below), its secular Yarkovsky-driven evolution is attracted by a particular value, for which the eccentricity derivative is positive.

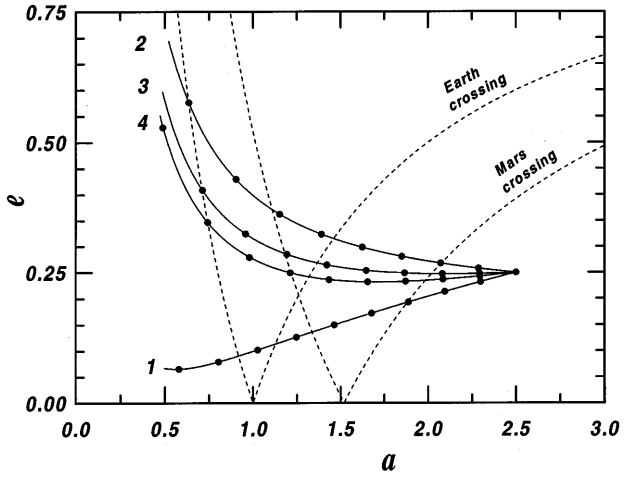

FIG. 5.—Yarkovsky-driven orbital evolution of fictitious basalt fragments in the a (semimajor axis in AU) vs. e (eccentricity) plane. Ticks correspond to intervals of 250 Myr for objects 50 m in radius; for smaller objects, evolutionary times would be shorter. Here the spin axis is assumed to lie in the orbital plane ($s_n = 0$), and we have used four different initial values of the pericenter longitude ϖ: (1) $\varpi = 0°$, (2) $\varpi = 45°$, (3) $\varpi = 90°$, and (4) $\varpi = 135°$. The Earth- and Mars-crossing curves are also shown (neglecting the planetary eccentricities).

4.3. *Planetary Perturbations and Spin Axis Precession*

An artificial feature of the previous examples of orbital evolution is that the pericenter longitude ϖ, and consequently the parameter $\hat{\omega}$, were assumed to drift very slowly due to the Yarkovsky perturbation only. Figure 6 shows the cumulative change $\delta\varpi(t) = \varpi(t) - \varpi(0)$ as a function of time for the four cases shown in Figure 5. However, there are at least two reasons why in reality ϖ and/or $\hat{\omega}$ undergo a rather fast circulation (with typical periods in the range 10^4–10^5 yr): (i) planetary perturbations on the orbit, and (ii) forced precession of the fragment's spin axis in the solar gravity field, leading to the corresponding changes in the $\hat{\omega}$ variable. As a consequence, the intervals of increase/decrease of the orbital eccentricity, corresponding to different values of $\hat{\omega}$, are rapidly following each other, and what matters is only the average evolution. We are now going to show that in this case the averaged trend is to slowly decrease the eccentricity. First we discuss the planetary perturbation terms in equations (28a)–(28c), while keeping constant the orientation of the fragment's spin axis, and then we include the spin axis precession.

4.3.1. *Planetary Secular Perturbations*

Remaining in the frame of a planar problem and identifying now the XY-plane with the mean ecliptic, we repeated our investigation of the combined secular planetary perturbations and the seasonal Yarkovsky effect on the motion of the asteroidal fragments, described in Vokrouhlický & Farinella (1998). Our analytical treatment of the planetary terms is based on the averaged perturbing potential developed to a very high order in the fragment's orbital eccentricity (15th order). In our previous work (Vokrouhlický & Farinella 1998), we considered only a very simple model for the thermal effects, namely, a secular change of the semimajor axis, whereas now we take into account all three equations (28a)–(28c) for the Yarkovsky perturbations of semimajor axis, eccentricity, and longitude of perihelion. Such a model is useful to describe accurately the strong perturbations affecting the orbital elements when the mean semimajor axis crosses the ν_6 secular resonance at the inner edge of the

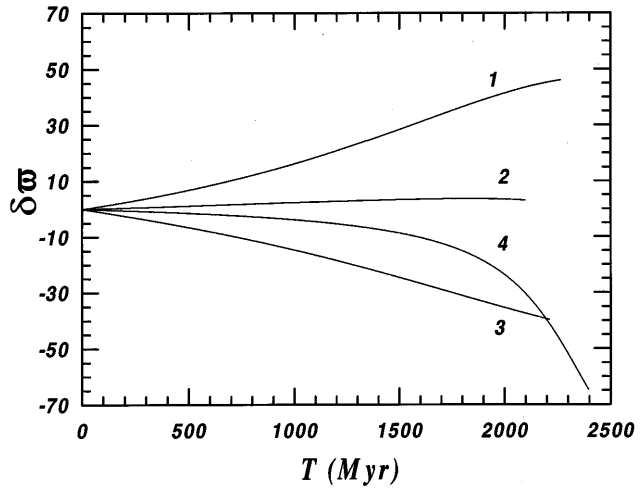

FIG. 6.—Yarkovsky-driven evolution of the argument of pericenter ϖ ($\delta\varpi = \varpi - \varpi_0$, where ϖ_0 is the starting value, in degrees) vs. time (in Myr). The four cases are the same shown in Fig. 5.

main asteroid belt (at this resonance, the rate of perihelion longitude becomes equal to the g_6 proper frequency of the planetary system). Of course, the semimajor axis is changed by the thermal effects alone, according to equation (28a).

In general, our current results agree well with those described in Vokrouhlický & Farinella (1998). As shown in Figure 7, when compared with the evolution illustrated in Figure 5, the main differences are (i) the high-frequency oscillations due to the planetary terms and (ii) the sudden eccentricity growth due to ν_6 resonance crossing (at a semimajor axis of about 2.10 AU). Apart from the resonance crossing, Figure 7 also shows an underlying very slow secular decrease of the mean eccentricity, due to the Yarkovsky effect. The time span of the integration is about 700 Myr, consistent with the Yarkovsky semimajor axis decay resulting from Figure 5.

It is also interesting to note that the Yarkovsky perturbation of the perihelion longitude is small enough not to affect significantly the position of the ν_6 resonance, which is mainly determined by the planetary terms. Quantitatively, according to Figure 6, the thermal perturbations contribute only $\approx 10^{-4}$ arcsec yr^{-1} to the perihelion precession rate, compared with about 27.5 arcsec yr^{-1} at the ν_6 resonance.

4.3.2. *Spin Axis Precession and Three-dimensional Orbits*

Let us briefly discuss the problem of the fragment's spin axis orientation, which so far has been assumed to lie in the orbital plane. In general, the spin axis undergoes a complex evolution that, if we leave aside the random component due to collisions, can be approximately split into to two different modes: (i) free precession and (ii) forced precession due to the solar gravitational torque.

First, we can estimate the typical periods for the two modes. Assuming a homogeneous spheroidal body having polar and equatorial radii $R_{A,p}$ and $R_{A,e}$ (with $\varepsilon = R_{A,p}/R_{A,e}$ as before), we obtain $(1-\varepsilon^2)/2$ for the dynamical flattening $\Delta \equiv (C-A)/C$ of the body (here C and A are the moments of inertia along the polar and equatorial axes). It follows that the ratio of the free-precession period $t_{\rm free}$ to the proper rotation period $t_{\rm rot}$ is approximately given by $t_{\rm free}/t_{\rm rot} \simeq 1/\Delta$ (Beletskii 1975). For a reasonable range of values of ε, we can estimate that the free precession period is at most of the order of a few days, even assuming that $t_{\rm rot}$ is as long as several hours. This timescale is much shorter than the averaging period of one revolution around the Sun. Therefore, the free precession mode can be neglected, simply by considering the averaged orientation of the spin axis (which coincides with the spin angular momentum vector) instead of its instantaneous orientation.

The situation is quite different in the case of the forced precession due to the solar gravity field. We can estimate its period $t_{\rm for}$ as $t_{\rm for} \approx \pi(t_{\rm rev}/t_{\rm rot})(t_{\rm rev}/\Delta)$, where $t_{\rm rev}$ is the orbital period, and obtain values of 10^5–10^6 yr for $t_{\rm for}$. These values are much longer than the averaging time $t_{\rm rev}$.

In order to assess the influence of the spin axis precession on the Yarkovsky orbital effects, we neglect the forced nutations and assume that the solar torque just causes $\boldsymbol{s}$ to precess uniformly around the normal to the mean orbit. In this case, ($d\boldsymbol{s}/dt \propto \boldsymbol{s} \times \boldsymbol{n}$), and using our variables we have

$$\gamma = \text{constant}\,, \tag{29a}$$

$$\frac{d\hat{\omega}}{dt} \simeq -\frac{3}{2}\frac{\Delta}{(1-e^2)^{3/2}}\frac{n^2}{\omega_{\rm rot}}\cos\gamma \tag{29b}$$

(e.g., Fitzpatrick 1970; Beletskii 1975). Here n is the orbital mean motion as before and $\omega_{\rm rot}$ is the rotational frequency. Assuming for instance $\Delta \simeq 0.1$, $t_{\rm rot} \simeq 3$ hr, and $e \simeq 0$, the resulting forced precession period is about 0.02 $a^3/\cos\gamma$ Myr.

We have integrated equation (29b) together with the system (17a)–(17c) for a fictitious body having $\Delta = 0.1$ and $t_{\rm rot} = 3$ hr. The initial orbital elements were $a = 2.5$ AU, $e = 0.25$, $I = 10°$, and $\Omega = \omega = 0$. The initial spin axis orientation was specified by $\gamma = 82.^\circ9$ and $\hat{\omega} = 135°$. Figure 8 shows the evolution of the orbit in the a versus e mean element plane. For the sake of comparison, we have also plotted the evolution assuming a constant spin axis orientation (note that in this case the parameters are very close to the case 2 integration of Fig. 5). The forced precession affects the evolution in two ways: (i) the eccentricity undergoes long-term oscillations with the precessional period (their amplitude is too small to be noticed in the scale of

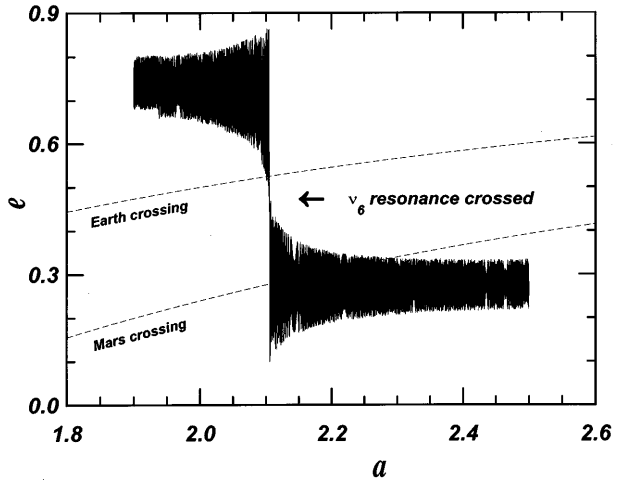

FIG. 7.—Effects of the secular planetary perturbations and the seasonal Yarkovsky force on the orbital evolution of a stony body 50 m in radius. As in Fig. 5, the evolution is shown in the a vs. e mean element plane. The initial conditions are the same as for curve 2 in Fig. 5, and the integration time span is about 700 Myr. The Earth- and Mars-crossing curves are also shown (*dashed lines*).

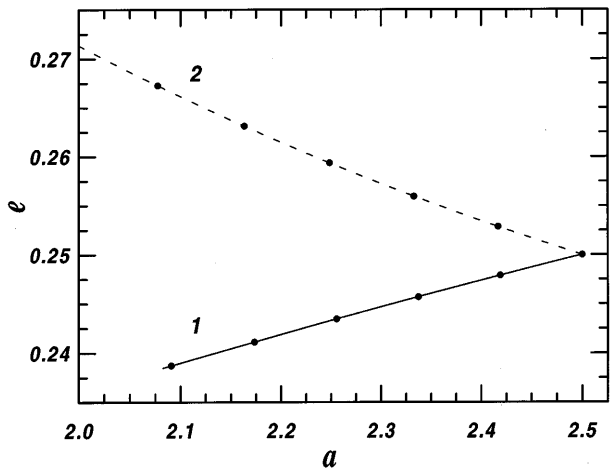

FIG. 8.—Yarkovsky-driven evolution of the mean orbital elements of a 50 m basalt fragment in the a (semimajor axis in AU) vs. e (eccentricity) plane. (1) The solid curve corresponds to a fragment whose spin axis undergoes the forced precession due to the solar torque and (2) the dashed curve to a fragment with a constant orientation of the spin axis. Ticks are at intervals of 100 Myr.

Fig. 8), and (ii) the eccentricity shows a secular decrease, instead of the increase found in the constant spin axis case. The latter result confirms our remark that, although for some values of $\hat{\omega}$ the mean eccentricity is pumped up by the thermal perturbation, the average over all possible values of $\hat{\omega}$ yields a net decrease of the eccentricity.

In this numerical example, we found that the inclination and the longitude of the node of the integrated orbit oscillate around their initial values. However, this is a peculiar case. When the planetary terms are considered together with the forced precession of the fragment's spin axis, the inclination, like the eccentricity, in general exhibits a slow change. Of course, sudden jumps may occur at resonance crossings, as discussed in Vokrouhlický & Farinella (1998).

5. CONCLUSIONS

The main results of this work can be summarized as follows:

1. We have developed a new nonlinearized model for the seasonal Yarkovsky effect acting on "large" bodies (i.e., in the plane-parallel approximation). By solving the corresponding equations with a numerical technique, we have found that the linear approximation of Rubincam (1995) leads to an overestimation of the rate of semimajor axis decay by about 15% for circular orbits.

2. Based on a generalization of our theory for spheroidal bodies, we estimate that nonspherical shapes of asteroid fragments can result in semimajor axis drift rates up to a factor of 2 faster or slower than in the spherical case. Vokrouhlický (1998b) reports a similar conclusion in the case of the diurnal Yarkovsky effect.

3. By introducing the seasonal Yarkovsky force in the Gaussian perturbation equations, we have found that for some orientations of the spin axis relative to the perihelion direction a secular increase of the eccentricity may arise. In the long term, if the spin axis were fixed and no other perturbation were present, the argument of perihelion would always be "attracted" to a value for which there is a secular eccentricity growth. On the contrary, according to the estimates from linearized models, Yarkovsky effects should always circularize orbits.

4. When the circulation of the argument of the pericenter due to planetary perturbations and/or the forced spin axis precession are taken into account, the mean secular effect on the eccentricity is a slow decrease. However, both for the eccentricity and for the inclination, secular perturbations are typically more important than Yarkovsky-driven effects, especially when the semimajor axis decay leads to a secular (or mean motion) resonance crossing.

A number of problems, not addressed in this paper, are open to further investigations. An obvious generalization of this work is to the "small body" case, when the depth reached by the seasonal thermal wave is comparable to or larger than the size of the body. We also need to better understand the interplay between Yarkovsky-driven secular effects and planetary perturbations, especially near or at secular and mean motion resonances. Finally, we need to develop realistic models for the evolution of fragments spin axes, in particular, under a flux of randomly oriented collisions by projectiles spanning a wide range of masses. On the observational side, we miss reliable estimates on the physical, thermal, and rotational properties of asteroid fragments in the 1–100 m size range, where the seasonal Yarkovsky effect is particularly important.

We are grateful to W. F. Bottke, W. K. Hartmann, F. Marzari, D. P. Rubincam, and S. J. Weidenschilling for useful discussions and comments. D. V. worked on this paper while staying at OCA/CERGA, Grasse (France). P. F. acknowledges partial support by the Italian Space Agency (ASI) and the Italian Ministry for University and Scientific Research (MURST).

REFERENCES

Afonso, G., Gomes, R. S., & Florczak, M. A. 1995, Planet. Space Sci., 43, 787
Beletskii, V. V. 1975, Motion of an Artificial Satellite about Its Center of Mass in Gravitational Field (in Russian) (Moscow: Moscow Univ. Press)
Bertotti, B., & Farinella, P. 1990, Physics of the Earth and the Solar System (Dordrecht: Kluwer)
Brown, R. H. 1985, Icarus, 64, 53
Brown, R. H., & Matson, D. L. 1987, Icarus, 72, 84
Burns, J. A., Lamy, P. L., & Soter, S. 1979, Icarus, 40, 1
Catullo, V., Zappalà, V., Farinella, P., & Paolicchi, P. 1984, A&A, 138, 464
Farinella, P., & Vokrouhlický, D. 1996, Planet. Space Sci., 44, 1551
Farinella, P., Vokrouhlický, D., & Hartmann, W. K. 1998, Icarus, 132, 378
Fitzpatrick, P. M. 1970, Principles of Celestial Mechanics (New York: Academic)
Giblin, I., Martelli, G., Smith, P. N., Cellino, A., Di Martino, M., Zappalà, V., Farinella, P., & Paolicchi, P. 1994, Icarus, 110, 203
Hartmann, W. K., Farinella, P., Weidenschilling, S. J., Ryan, E. V., Vokrouhlický, D., Marzari, F., Spaute, D., & Davis, D. R. 1997, in Proc. Lunar and Planet. Sci. Conf. 28 (Houston: Lunar Planet. Inst.), 517
Kaula, W. M. 1966, An Introduction to Planetary Physics (New York: Wiley)
Lagerros, J. S. V. 1996, A&A, 310, 1011
Landau, L. D., & Lifschitz, E. M. 1986, Hydrodynamics (Moscow: Nauka)
Lebofsky, L. A., & Spencer, J. R. 1989, in Asteroids II, ed. R. Binzel, T. Gehrels, & M. S. Matthews (Tucson: Univ. Arizona Press), 128
Milani, A., Nobili, A. M., & Farinella, P. 1987, Non-gravitational Perturbations and Satellite Geodesy (Bristol: Hilger)
Öpik, E. J. 1951, Proc. R. Irish Acad., 54, 165
Peterson, C. 1976, Icarus, 29, 91
Rabinowitz, D. L. 1993, ApJ, 407, 412
———. 1994, Icarus, 111, 364
Radzievskii, V. V. 1952, AZh, 29,162
Rubincam, D. P. 1987, J. Geophys. Res., 92, 1287
———. 1988, J. Geophys. Res., 93, 13,805
———. 1995, J. Geophys. Res., 100, 1585
———. 1998, J. Geophys. Res., 103, 1725
Slabinski, V. J. 1997, Celest. Mech. Dyn. Astron., 66, 131
Spencer, J. R., Lebofsky, L. A., & Sykes, M. V. 1989, Icarus, 78, 337
Vokrouhlický, D. 1998a, A&A, 335, 1093
———. 1998b, A&A, in press
Vokrouhlický, D., & Farinella, P. 1998, A&A, 335, 351
Wesselink, A. J. 1948, Bull. Astron. Inst. Netherlands, 10, 351
Yomogida, K., & Matsui, T. 1983, J. Geophys. Res., 88, 9513